climate

MDPI

Article

Precipitation Trends and Flood Hazard Assessment in a Greek World Heritage Site

Elias Dimitriou

Hellenic Centre for Marine Research—H.C.M.R., Institute of Marine Biological Resources and Inland Waters, 19013 Anavyssos, Greece; elias@hcmr.gr

Abstract: Natural disasters have become more frequent and intense over the last decade mainly as a result of poor water and land management. Cultural sites and monuments are extremely vulnerable to natural disasters, particularly floods, while mitigation measures and protective infrastructure are difficult to construct within such areas. In the present study, the precipitation trends of the recent past and over the next 80 years were analyzed for the old town of Corfu (UNESCO World Heritage Site) in order to identify potentially significant changes that may affect the flood risk of the area. Moreover, a multi-criteria analysis using GIS software was used to identify high flood hazard zones in this living monument in order to propose specific mitigation measures that are in line with the characteristics of the site. The main effort in this study was to find a methodological approach for a fast but reliable assessment of future changes in the flood risk of historic monuments without the need for a hydrodynamic model and with a limited amount of locally based data. With the selected approach, a good indication of the potential changes in flood risk was provided, according to climate scenarios and simple, physically-based geostatistical models. The results indicate that no significant changes in the flood risk were found for the future climatic conditions, and the identified flood-prone areas will remain approximately the same as today in this particular historic monument. The uncertainty that is included in this output originates mainly from the inherent errors in climate modeling and from the non-high temporal resolution of the data.

Keywords: Corfu Old Town; flood hazard; risk assessment; cultural monuments; World Heritage Site

check for updates

Citation: Dimitriou, E. Precipitation Trends and Flood Hazard Assessment in a Greek World Heritage Site. *Climate* **2022**, *10*, 194. https://doi.org/10.3390/cli10120194

Academic Editors: Lavinia de Ferri and Mohammad Valipour

Received: 19 September 2022
Accepted: 1 December 2022
Published: 5 December 2022

1. Introduction

Natural disasters have appeared with higher frequency during the last decades due to extreme climatic events and poor land and water management practices [1]. This has had detrimental impacts on the environmental and socioeconomic status in many countries, while archaeological and cultural heritage areas are even more vulnerable to these threats [2,3]. Moreover, mitigating the impacts of natural disasters on protected cultural sites is a very difficult task since the potential for interventions and constructions in these areas are limited and under significant restrictions [4]. Therefore, estimating the potential flood risk with improved accuracy and designing small-scale, efficient mitigation measures is a challenging but essential task [5]. The present research effort aims to assess the flood risk under current and future climatic scenarios, in the old town of Corfu island, which was designated as a 'World Heritage Site' by UNESCO in 2007 and has an area of approximately 1 km^2 (Figure 1). The old town of Corfu is a living monument (it is nowadays inhabited), which includes an urban area and a port built in the 8th century B.C. and further developed during the 19th century by the Venetians [6]. There are two castles (one Byzantine and one Venetian) on the periphery of the town, which receive very large numbers of visitors every year. Several flood events have been observed in the past, caused by stormwater, without significant damages. However, due to the possible intensification of extreme weather events under future climatic variations, the flood risk in this living monument should be carefully assessed.

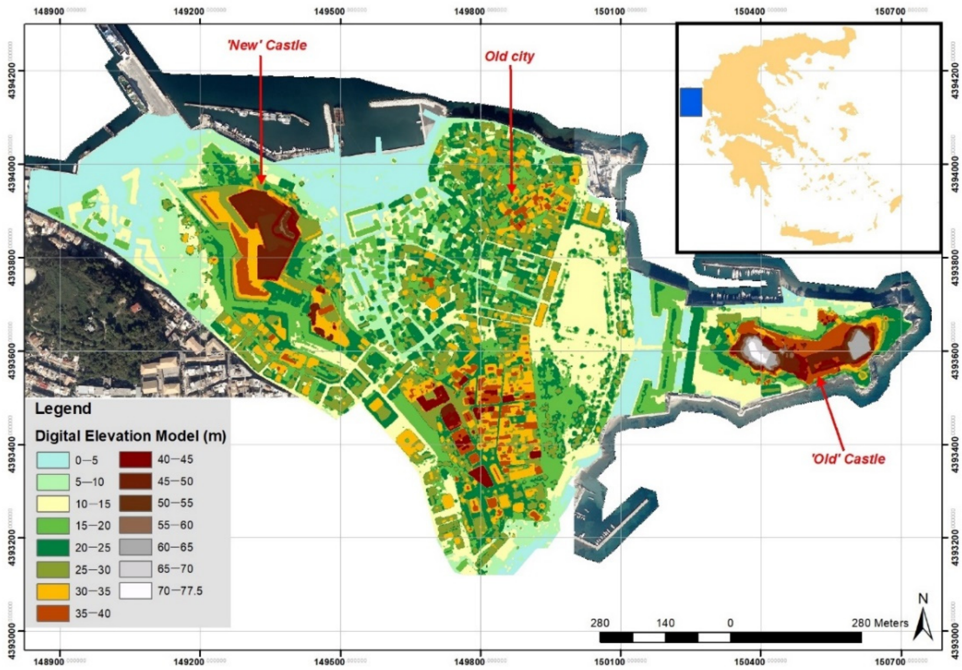

Figure 1. Topographic map of Corfu Old Town and the castles (coordinate system of the map is GGRS87 (Greek Geodetic Reference System, the center of the study area in WGS84 is: Lat.:39.6240, Long.: 19.9218).

Therefore, in this study, an analysis of the precipitation trends in the study area in the recent past (1971–2004) and under different climatic scenarios (Intergovernmental Panel for Climate Change (IPCC): 2031–2060 and 2061–2098) was conducted to identify potential changes in the future flood risk and propose relevant mitigation measures.

Hydrodynamic models can be used [1] to estimate flood risk, but the lack of hydrologic measurements and very detailed topographic data needed impose other alternatives, such as GIS-based multi-criteria risk assessment models [5]. The particularity of the study area is that it is an old and protected urban area, densely populated and with very narrow streets in which a very detailed topographic survey was not possible. Thus, applying a hydraulic model for the flood risk assessment was not feasible. Therefore, a multi-criteria analysis of the geospatial and hydrometeorological factors was implemented using GIS software and an analytic hierarchy process (AHP) model [5] to identify the high-hazard areas and estimate the flood risk potential in the study area.

Liu [2] applied a similar approach to extract historical floods at the Angkor monument in Cambodia, focusing on four indices (flood-affected frequency, absolute elevation, elevation standard deviation, and drainage density), and efficiently identified the flood-prone areas. In addition, Ortiz [3] applied a flood hazard assessment in the protected city of Merida in Spain by implementing vulnerability mapping and an analytic hierarchy process model, which was proven to be an efficient and cost-effective approach. Mentzafou [5] used exactly the same methodological steps as the present effort to map the flood hazard in a large transboundary river basin with satisfactory accuracy, which was assessed by comparing the high-hazard areas with past flood extents. This approach allows for the prioritization of the different hazard types in order to facilitate decision-making processes for developing mitigation infrastructure.

Therefore, an additional effort of this study was to identify and test a methodological approach for a fast and reliable assessment of flood-risk changes in historic monument areas that have a limited availability of data and important intervention restrictions for both acquiring new data and applying mitigation measures at a later stage.

2. Materials and Methods

A statistical analysis of the existing precipitation data from past measurements (1971–2004) and future climate change scenarios (2031–2060 and 2061–2098, IPCC, [7]) was conducted to identify potential increasing trends that could affect the flood risk. Then, an intensity index for precipitation was estimated (modified Fournier index (MFI) [8]), and its temporal trends were presented, while the flood risk maps for the current and future periods were estimated according to Kourgialas and Karatzas [9]. A comparative assessment of the outputs followed to identify the hotspots of flood risk in the old town of Corfu and evaluate the impacts that climate change may have on the area.

2.1. Precipitation Data

The precipitation data used in the present study came from the regional climate model RACMO22E (regional climate model of the Royal Netherlands Meteorological Institute (KNMI) driven by the HadGEM-ES of the Met Office Hadley Center global climate model (RACMO22e-MOHC)) with a spatial resolution of about 12 km (0.11°). The data concern three periods, namely (a) the reference period: 1971–2004, (b) the near future period: 2031–2060, and (c) the far future period: 2069–2098. The climate projections (daily data) were based on the climate scenarios RCP 2.6 (strict mitigation scenario), RCP 4.5 (intermediate mitigation scenario), and RCP 8.5 (extreme or very high emissions, IPCC: fifth assessment report, [7]). The data were downloaded from https://hypeweb.smhi.se/explore-water/climate-change-data/europe-climate-change/ (accessed on 4 May 2022).

2.2. Precipitation Trends and Statistical Analysis

Statistical analysis was performed on the precipitation data in statistical processing software (STATISTICA) in order to obtain possible trends of the amount and intensity of rain on daily, monthly, and annual levels for the study periods (1971–2004, 2031–2060, and 2069–2098).

Time-series statistics (mean value, median, maximum–minimum values, 25th and 75th percentages) and annual trend lines were also calculated, and the distribution of the annual precipitation values is presented in a histogram.

For the monthly values, the percentage deviations in the average monthly precipitation values of the future periods from the respective values of the reference period were calculated, while comparative box-plots were created with the monthly precipitation fluctuations for each scenario (expressed as the median, 25th–75th percentiles, and max–min values).

The intensity of precipitation was calculated using the modified Fournier index, which expresses the sum of the average monthly rainfall aggressiveness index at a location (Morgan, 2005):

$$MFI = \sum_{1}^{12} \frac{p^2}{P} \tag{1}$$

where *MFI* is the modified Fournier index, p is the average monthly rainfall (mm), and P is the average annual rain (mm). The *MFI* classes are as follows: low rainfall aggressiveness: <100, moderate aggressiveness: 100–300, high aggressiveness: 300–400, and very high aggressiveness: >400.

The *MFI* index was calculated for each year for the whole study period (1970–2098) in order to estimate possible future trends in the rainfall aggressiveness index due to climate change. Frequency distribution diagrams of the *MFI* index were created for each climate scenario and compared to the reference period, while a corresponding box-plot showing the variations in the *MFI* index for each scenario was produced.

2.3. Flood Risk Map Assessment

An assessment of the high-flood hazard and risk areas of the study area was carried out with the methodology developed by Kourgialas and Karatzas [9]. Based on this approach, a flood hazard map was produced after integrating a multicriteria factor analysis with GIS software in a very detailed grid cell (about 1 × 1 m).

More specifically, six individual raster maps were created for each of the main factors that contribute to the development of floods. These factors were: flow accumulation, slope, land-use types, rainfall aggressiveness, geology, and elevation of the study area. The impact of each factor was rated in five different risk categories: very high, high, moderate, low, and very low. In the case of numerical factors (flow accumulation, slope, altitude, and rainfall aggressiveness), the hazard classes were defined by Jenk's natural breaks method, while in cases of non-numerical factors (geology and land use), the risk classification was defined following subjective criteria, depending on their influence on flood processes (Table 1). Jenk's natural breaks method is a data classification method designed to optimize the arrangement of a set of values into 'natural' classes. This classification method seeks to minimize the average deviation from the class mean while maximizing the deviation from the means of the other groups. The method reduces the variance within classes and maximizes the variance between classes. It is also known as the goodness of variance fit (GVF), which equals the subtraction of the sum of squared deviations for class means (SDCM) from the sum of squared deviations for array mean SDAM.

Table 1. Flood hazard factors and their characteristics, adapted from Kourgialas and Karatzas [9].

No	Factor	Value Variation	Risk of Flooding	Factor Subweight (w)	Factor Gravity (x)	Factor (w×x)	Total Weight	Total Weight (%)
1	Flow concentration	>1762	Very high	10	2	20	52	14.6%
		844–1762	High	8		16		
		322–844	Moderate	5		10		
		73–322	Low	2		4		
		0–73	Very low	1		2		
2	Slope (degrees)	0–3.0	Very high	10	1.5	15	39	11.0%
		3.0–8	High	8		12		
		8–14	Moderate	5		7.5		
		14–50	Low	2		3		
		>50	Very low	1		1.5		
3	Land use	Coastal zones	Very high	10	4.5	45	117	32.9%
		Shrubland/meadows	High	8		36		
		Intensive Crops	Moderate	5		22.5		
		Non-intensive crops	Low	2		9		
		Mixed vegetation zone	Very low	1		4.5		
4	MFI	>400	Very high	10	1.5	15	39	11.0%
		300–400	High	8		12		
		200–300	Moderate	5		7.5		
		100–200	Low	2		3		
		100<	Very low	1		1.5		
5	Geology	Quaternary sediments	Very high–High	9	2	18	31	8.7%
		Neogene sediments	Moderate	5		10		
		Rock formations	Low–Very low	1.5		3		
6	Altitude (m)	0–8	Very high	10	3	30	78	21.9%
		8–18	High	8		24		
		18–27	Moderate	5		15		
		27–40	Low	2		6		
		>40	Very low	1		3		
			Total				356	100.0%

Each factor was then assigned a weighting factor, again depending on its influence on flood processes in this particular basin. Finally, the flood hazard map was created after the algebraic summation of each weighted factor [10] according to the following equation:

$$S = \sum_{1}^{i} w_i \times x_i \tag{2}$$

where S is the weighted hazard index, w_i is the weight of factor i, and x_i is the relative importance of factor i.

The inundation areas can be determined indirectly from the accumulation of a flow map [11], which was created in a GIS environment using a flow direction map generated from a digital elevation model (DEM) of the study area (acquired from the Hellenic Cadastre SA with a cell size of 1 m).

Terrain slopes and elevations were calculated using ArcMap software by using the digital elevation model (DEM) and the respective toolbox, while land uses were derived from the European land use coverage system CORINE 2018. The geology was described from the corresponding geological map (scale 1:50,000) acquired from the Institute of Geological and Mineralogic Exploration (IGME).

Both the average and maximum MFI values were used for the reference (1971–2004) and the future periods (2031–2060 and 2061–2098) to assess the flood hazard (development of an average and a maximum flood hazard map for each period). Then, the hazard maps were combined in ArcMap software with the significance of possible impacts (combination of vulnerability and exposure) due to a flood occurrence in the study area. However, since the case study area is the old city of Corfu, which is a UNESCO monument, the significance of potential damages and impacts were considered equally high in the urban part of the old city and low for the natural areas. Thus, the damage scores are flat-rate increases in the risk score of 20% in the case of urban areas and of 3% for natural and open areas. These figures are the result of testing in different case study areas, and the main purpose is to emphasize the flood hazard in areas that are more vulnerable. These values were applied homogeneously to all scenarios, and therefore, had the same impacts on each flood risk map. Thus, for urban areas, the highest impact was given (the hazard score was multiplied by 1.2), while for areas that were mainly green spaces or natural areas, a low impact index was provided (the hazard score was multiplied by 1.03). The adjustment to the flood hazard index, by considering the potential impacts, produced the flood risk maps for each period, which indicates the areas that should be a priority in terms of mitigation measures for flood protection.

3. Results

3.1. Precipitation Trends

Corfu is one of the regions with the highest annual rainfall in Greece, exceeding 1200 mm on average over the period of 1950–2020 [12]. In order to assess the validity of the rainfall data from a regional climate model with respect to the actual rainfall conditions on the island of Corfu, a comparative analysis was realized using the rainfall data from the Corfu airport station and the climate model output for the period of 1971–2004 (daily values). The comparison indicated that approximately the lowest 50% of the rainfall values are similar using the two different sources (model and gauging station), while the model tended to overestimate the rainfall values in the range between the median and the 75th percentile (Figure 2). This was partially due to some periods of malfunctioning at the station, which, in an operational duration of 33 years (1971–2004), are unavoidable. Moreover, the estimated differences are not very high, and thus, the model seems consistent with the local climatic conditions of the study area. This is also accredited by the average monthly values for the aforementioned period that present a very high coefficient of determination (R2 = 0.96).

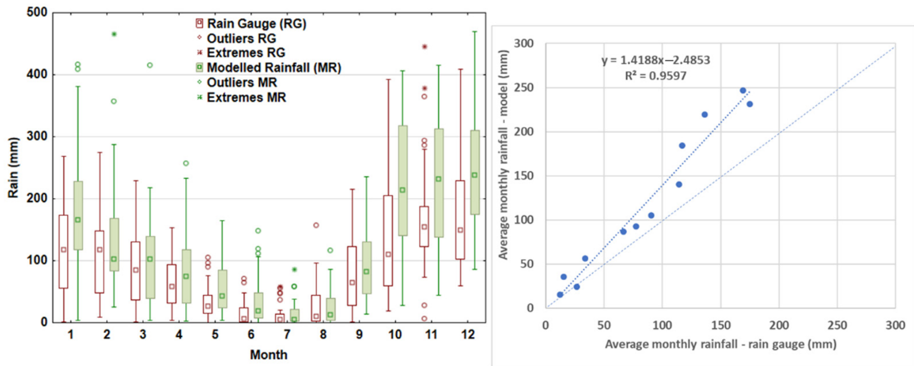

Figure 2. Comparison of monthly rainfall values from a rain gauge at Corfu airport and from the RACMO22E climate model for the period of 1971–2004.

Based on the statistics of the data available for this study, it appears that in the reference period (1971–2004), the average annual rainfall was 1438 mm, while the corresponding figures are also observed in the climate scenarios, with the exception of the RCP 2.6 and RCP 4.5 scenarios for the period of 2031–2060, which show slightly higher rainfall heights (1532 and 1531 mm, respectively, Table 2).

Table 2. Basic annual precipitation statistics for the reference period and climate scenarios.

	1971–2004	RCP 2.6 /2031–2060	RCP 2.6 /2061–2098	RCP 4.5 /2031–2060	RCP 4.5 /2069–2098	RCP 8.5 /2031–2060	RCP 8.5 /2069–2098
Average	1437.9	1532.3	1482.7	1530.9	1427.3	1467.1	1381.2
Median	1385.3	1546.1	1391.2	1539.0	1489.1	1439.4	1310.9
Min	785.0	832.6	1049.9	1031.8	983.2	725.8	737.7
Max	2328.0	2048.9	2184.3	2214.4	2009.3	2380.9	1932.5
25th percentile	1292.2	1428.1	1239.7	1324.9	1266.2	1165.8	1175.4
75th percentile	1583.0	1690.5	1681.8	1714.2	1579.3	1701.6	1683.1

The maximum annual rainfall during the reference period reached 2328 mm, while in all climate scenarios, the corresponding amount is smaller, with the exception of the RCP 8.5 scenario for the period of 2031–2060, which presents a maximum annual rainfall of 2381 mm.

On average, there are slightly decreasing trends in precipitation in the climate scenarios for the period of 2031–2060 (Figure 3), while in the frequency distribution of annual precipitation, significant percentages of the values of the RCP 45 and RCP 85 scenarios (20 and 23% of the totals, respectively) have lower precipitation values (between 1000 and 1200 mm) compared to the period of 1971–2004 (6% of values range between 1000 and 1200 mm, Figure 4). Nevertheless, a relatively high percentage of annual values range between 1400 and 1800 mm in the RCP 2.6 scenario (73%), in contrast to the reference period when precipitation values in this range (1400–1800 mm) are 42% of the total (Figure 4). In the very high precipitation ranges (above 1800 mm) the RCP 8.5 scenario presents the highest percentage of values exceeding this threshold (23% of the total) compared to the reference period (6%).

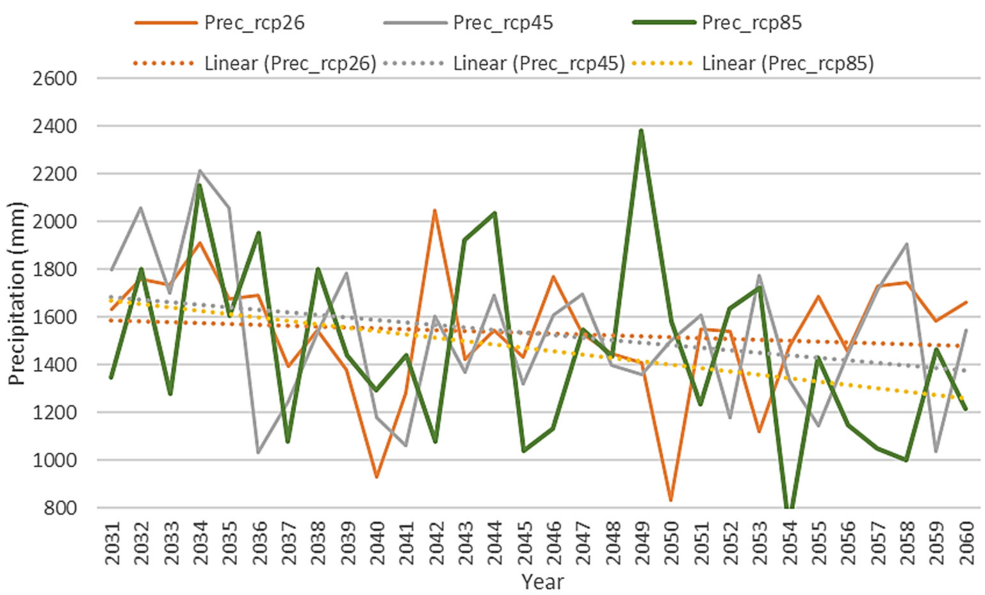

Figure 3. Annual precipitation values for the period 2031–2060 for the 3 climate scenarios.

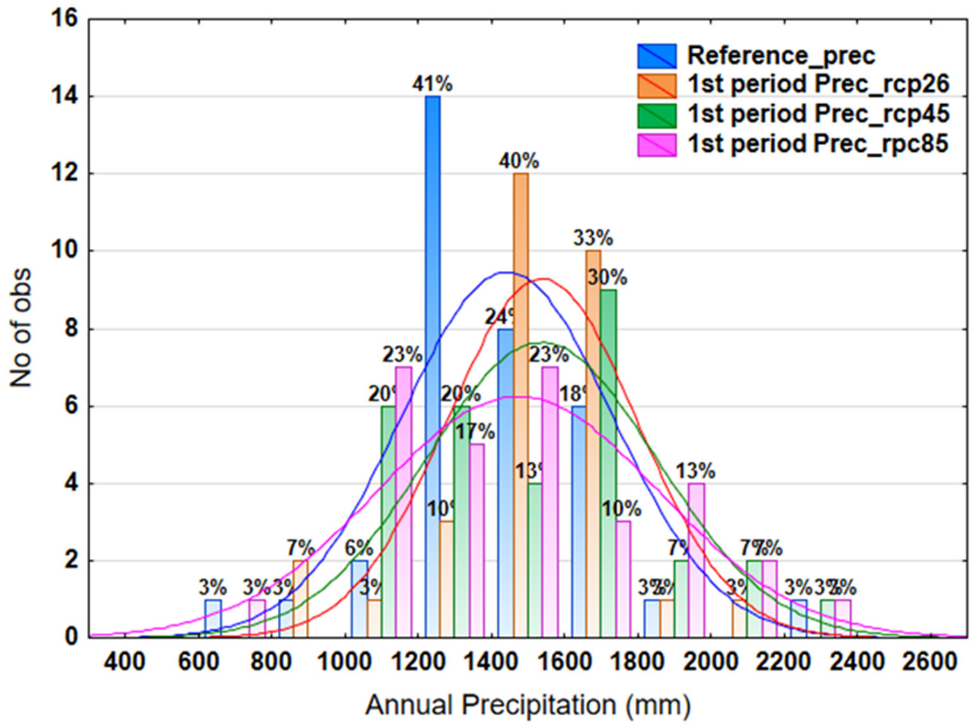

Figure 4. Frequency distribution of annual rainfall for the reference period and the 3 climate scenarios of the first study period (2031–2060).

In the second study period (2061–2098), a very small increasing trend in the annual precipitation is observed for the RCP 2.6 and RCP 4.5 scenarios, but it is not statistically significant (Figure 5). Regarding the distribution of the annual values, there are no significant differences between the reference period and the climate scenarios with the exception of very high precipitation values (over 1800 mm), where, in the RCP 2.6 and RCP 8.5 scenarios, 17% and 13% of the values exceed this threshold, while in the reference period, only 6% of the annual precipitation values fall within this range (Figure 6).

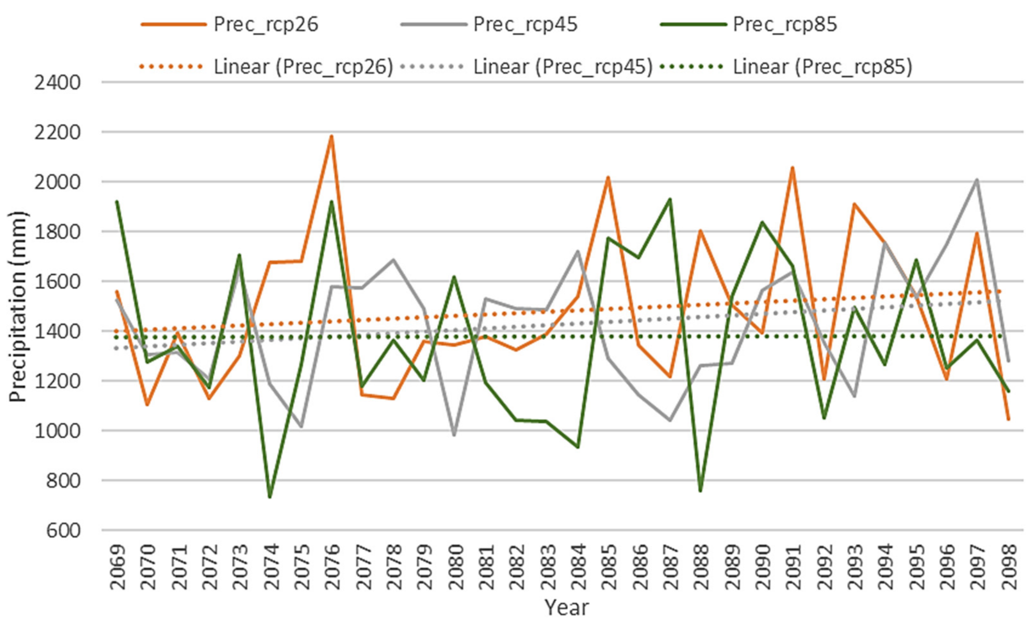

Figure 5. Annual precipitation values for the period of 2061–2098 for the 3 climate scenarios.

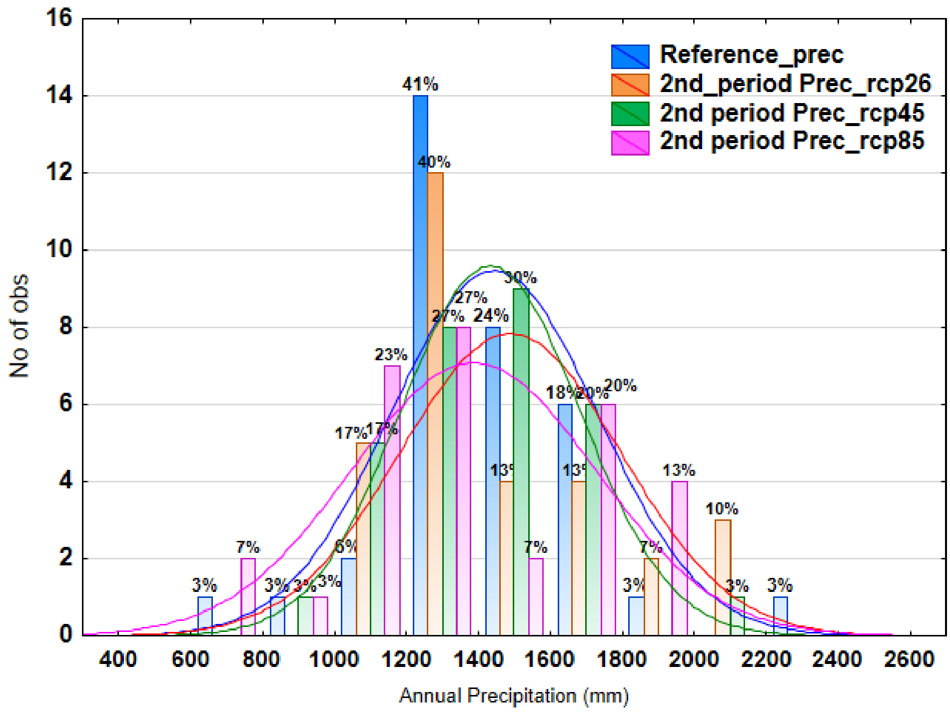

Figure 6. Frequency distribution of annual rainfall for the reference period and the 3 climate scenarios of the second study period (2061–2098).

Regarding the average monthly rainfall values, the months of October, November, and December present the highest values during the reference period (219–247 mm), while in the remaining months, the average monthly values do not exceed 184 mm for the reference period. The monthly values in the climate scenarios are also similar, with small differences compared to the reference period that are within the limits of the statistical error (Table 3).

Table 3. Average monthly precipitation values for the reference period and climate scenarios.

Months	1971–2004	RCP 2.6 /2031–2060	RCP 2.6 /2061–2098	RCP 4.5 /2031–2060	RCP 4.5 /2069–2098	RCP 8.5 /2031–2060	RCP 8.5 /2069–2098
1	184.11	239.06	243.88	220.98	194.60	217.25	221.54
2	139.98	166.63	178.16	153.43	172.23	143.81	129.16
3	105.45	89.84	100.85	89.73	121.50	99.88	120.12
4	86.82	87.52	77.08	77.95	85.71	78.99	69.65
5	56.20	81.69	57.67	70.09	50.36	66.03	40.84
6	35.81	41.44	50.76	32.40	43.25	39.07	34.86
7	15.27	10.11	16.35	9.47	16.00	9.51	9.67
8	24.55	22.92	30.15	24.64	38.40	33.01	39.66
9	92.66	109.42	120.88	105.70	104.57	85.36	106.47
10	219.44	209.41	173.90	212.30	213.07	219.04	200.54
11	231.03	256.70	242.88	285.80	222.87	262.80	203.78
12	246.57	217.54	190.19	248.38	164.72	212.33	204.88

Based on the average percentage differences in the average precipitation values of the climate scenarios in relation to the reference period, there are some significant increasing trends in the months of August and May (between 40 and 60% in relation to the corresponding values of the reference period), while the remaining values do not illustrate significant differences in relation to those of the reference period (Figure 7).

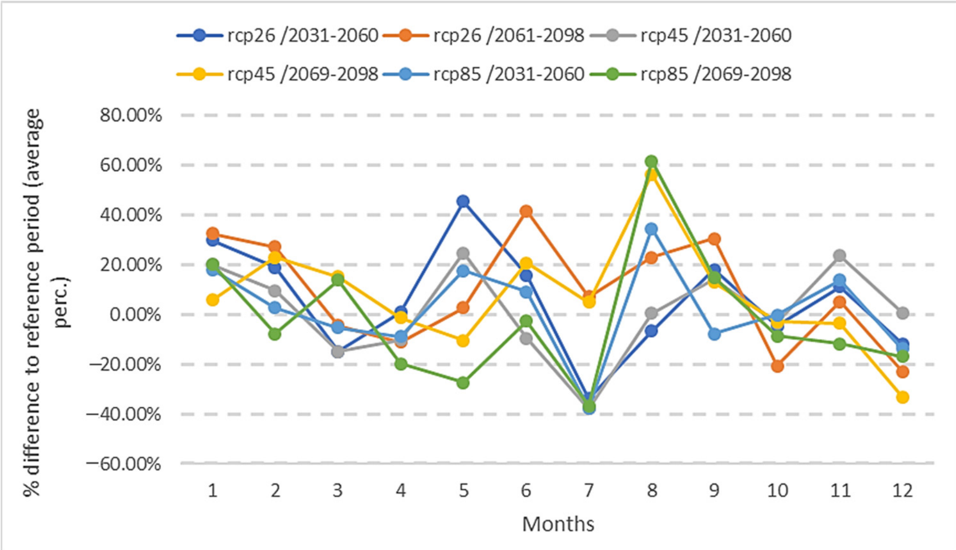

Figure 7. Percentage differences in average monthly rainfall for all climate scenarios relative to the average monthly rainfall in the reference period.

Regarding the mean maximum monthly precipitation values, the highest values are observed in the months of December, January, and February, ranging from 416 to 469 mm for the reference period (Table 4). In the remaining months, the maximum monthly rain values are significantly lower (below 256 mm for the reference period), while the monthly maximum precipitation levels in the climate scenarios are similar. Nevertheless, some particularly increased monthly maximum rainfall for the month of October was observed in the climate scenarios RCP 4.5 and RCP 8.5 for the period of 2069–2098 (from 561 mm to 665 mm) and in RCP 8.5 for the period of 2031–2060 (568–871 mm, Table 4).

Table 4. Maximum monthly precipitation values for the reference period and climate scenarios.

Months	1971–2004	RCP 2.6 /2031–2060	RCP 2.6 /2061–2098	RCP 4.5 /2031–2060	RCP 4.5 /2069–2098	RCP 8.5 /2031–2060	RCP 8.5 /2069–2098
1	416.62	534.12	448.63	507.95	552.38	405.74	506.07
2	465.78	426.92	462.50	352.93	387.32	358.30	397.69
3	415.37	229.96	184.01	242.21	363.33	313.45	418.19
4	256.58	228.53	224.50	215.50	203.59	192.53	302.39
5	164.61	233.94	181.44	330.16	280.02	236.27	153.49
6	148.15	164.06	187.13	138.98	213.40	133.17	161.76
7	86.35	35.88	65.25	67.34	72.79	49.73	70.02
8	116.95	89.58	135.42	102.31	146.17	342.12	173.33
9	235.84	395.27	295.53	263.76	282.45	373.70	280.31
10	406.03	453.55	375.05	452.77	**561.90**	**566.68**	**664.73**
11	415.25	602.79	537.09	509.42	**518.49**	**871.11**	427.28
12	469.39	404.65	473.78	596.42	431.27	509.62	491.45

In terms of the percentage differences in the maximum monthly values of precipitation for each climate scenario in relation to the reference period, no substantial trends are observed, with the exception of the month of August in the scenario RCP 2.6 (2031–2060), where the average maximum value of rainfall is approximately 200%greater than that of the reference period, (Figure 8).

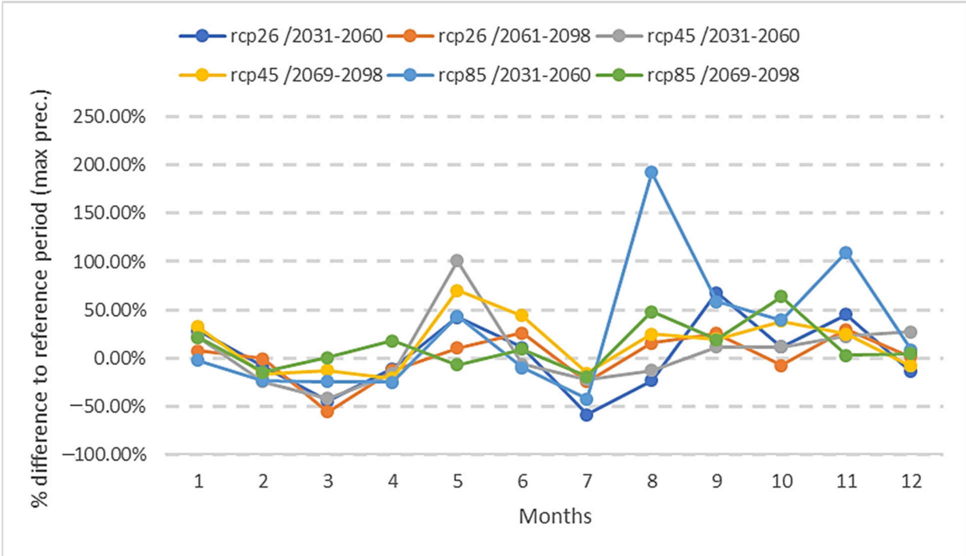

Figure 8. Percentage differences in mean maximum monthly rainfall for all climate scenarios relative to reference period mean maximum monthly rainfall.

The box-plot diagrams of the maximum monthly precipitation values also indicate that there are no significant differences between the reference period and the climate scenarios of the first period (2031–2060), with the exception of some very high values observed mainly in the RCP 2.6 and RCP 8.5 scenarios in the months of October and November (Figure 9).

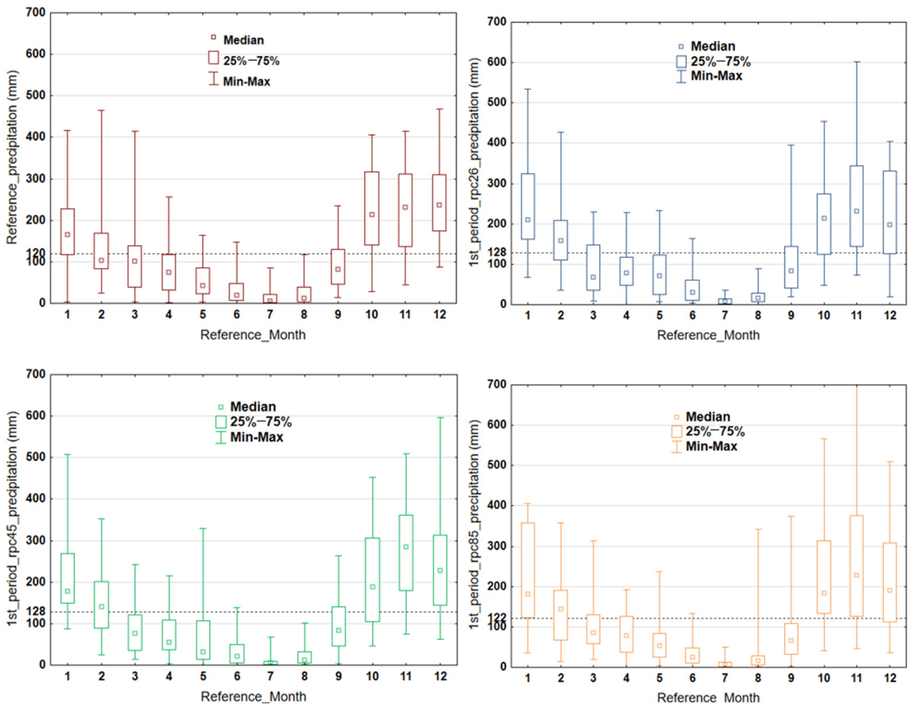

Figure 9. Distribution of the variations in the maximum monthly precipitation values for the reference period and the first-period climate scenarios (2031–2060). Dashed lines are the average values of the projected data.

Similarly, the differences in the maximum monthly precipitation values between the reference period and the climate scenarios of the second period (2069–2098) are smaller than those mentioned above for the climate scenarios of the first period, with the exception of the month of November and scenarios RCP 2.6 and RCP 4.5 (Figure 10).

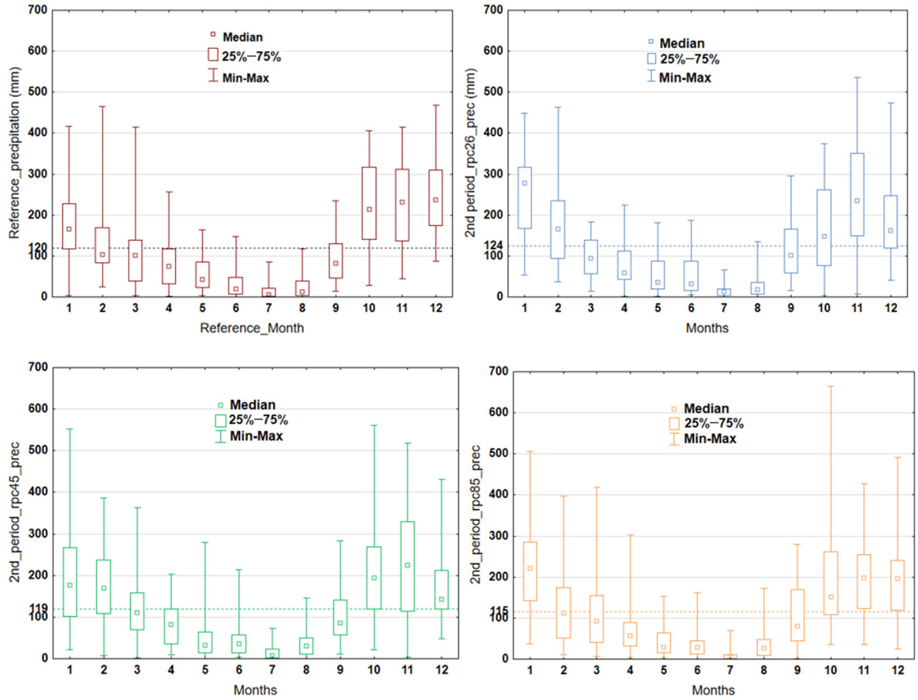

Figure 10. Distribution of the variations in the maximum monthly precipitation values for the reference period and the second-period climate scenarios (2069–2098). Dashed lines are the average values of the projected data.

The daily precipitation values in the reference period and in the climate scenarios of both study periods (Figures 11 and 12) are below 100 mm, while no significant differences between the reference period and the climate scenarios exist. In the first period (2031–2060) and the RCP 2.6 scenario, slightly more values of above 100 mm are observed compared to the reference period, while in the RCP 8.5 scenario, an extreme precipitation value approaching 300 mm is observed (Figure 11).

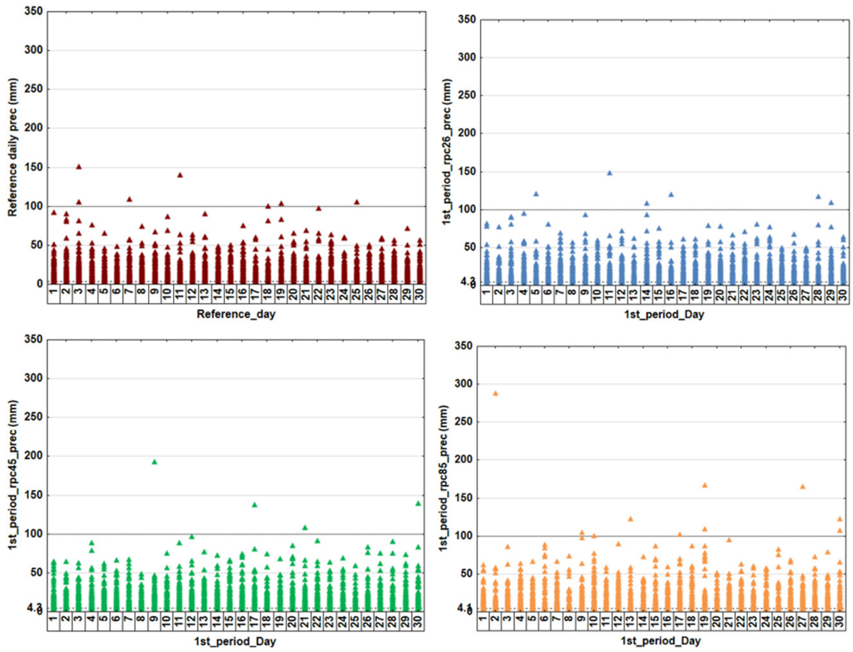

Figure 11. Fluctuations of daily precipitation values for the reference period and the climate scenarios of the first period. Dashed lines are reference lines for comparative purposes.

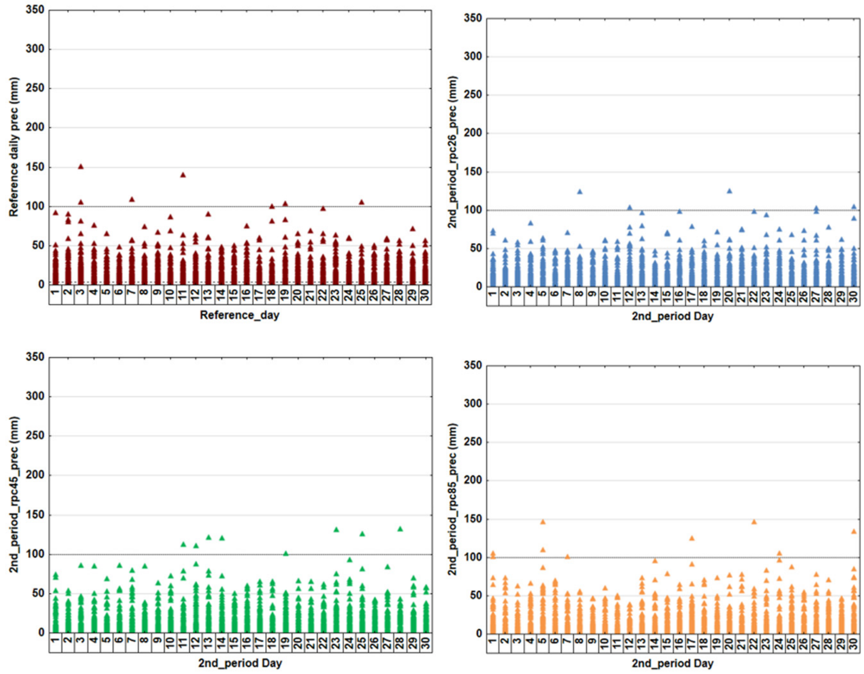

Figure 12. Fluctuations of daily precipitation values for the reference period and the climate scenarios of the second period. Dashed lines are reference lines for comparative purposes.

In the second study period (2069–2098), smaller differences in the daily precipitation levels are observed between the reference period and the climate scenarios (Figure 12).

3.2. MFI Index

The MFI index expresses the aggressiveness of precipitation per year and is considered high when it exceeds a value of 300 [13]. In the study area, the MFI ranges between 68 and 506 for the reference period and shows significantly higher values only in the RCP 8.5 climate scenario during the period of 2031–2060 (ranging from 56 to 779, Table 5). The average values of the index do not show significant variations between the reference period and the climate scenarios.

Table 5. MFI statistics for the reference period and climate scenarios.

	Reference Period	1st Period RCP 26	1st Period RCP 45	1st Period RCP 85	2nd Period RCP 26	2nd Period RCP 45	2nd Period RCP 85
Average	220.93	240.87	256.28	258.02	231.98	227.75	235.29
Max	506.10	512.13	586.73	778.99	437.71	502.18	508.79
Min	68.02	74.91	109.97	56.40	112.64	104.71	52.74
Median	206.56	220.68	251.29	241.12	205.71	215.55	206.10
25th percentile	173.78	184.51	155.77	141.42	160.79	152.45	156.42
75th percentile	260.59	283.35	312.82	313.32	301.86	275.10	309.56

Regarding the distribution of the MFI values, in the reference period, most values ranged between 100 and 300 (medium aggressiveness), while during the first period (2031–2060) of the climate scenarios, significantly more high values (above 300) are presented in all scenarios, with the RCP 8.5 scenario showing several values above 400 (very high rain aggressiveness, Figure 13).

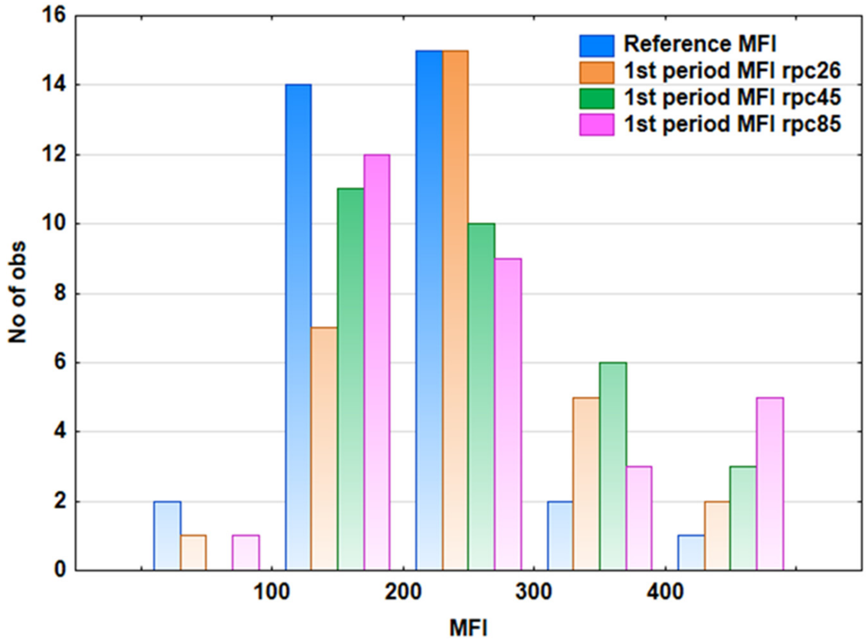

Figure 13. Distribution of MFI values in the reference period and the first-period climate scenarios.

A similar distribution is also observed in the second period of climate scenarios (2069–2098), with all scenarios showing more 'high and very high' MFI values compared to the reference period, while at the same time, an increase in low MFI values (below 200) is also observed in the climate scenarios in relation to the reference period (Figure 14).

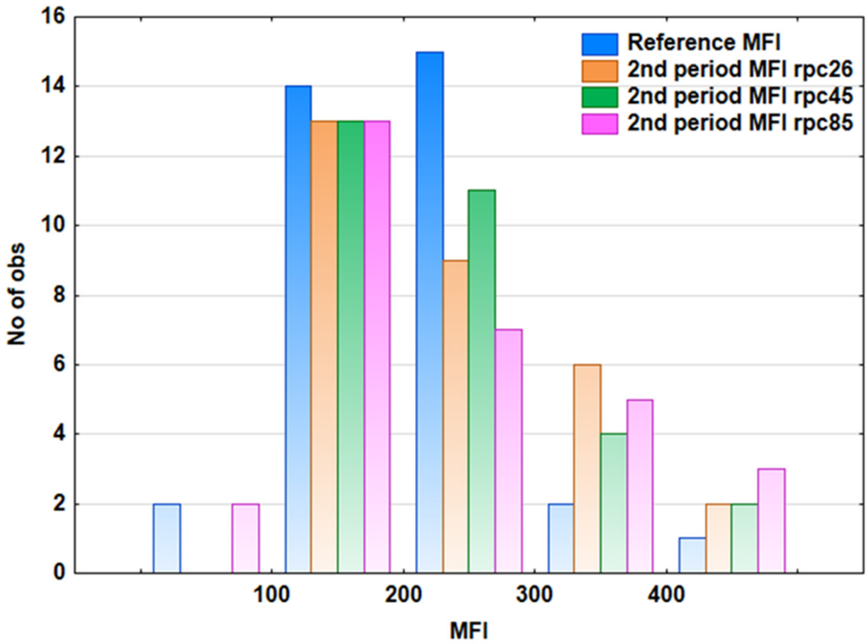

Figure 14. Distribution of MFI values in the reference period and the second-period climate scenarios.

The variation in the MFI index for the reference period (1971–2004) is slightly smaller than the MFI index in the climate scenarios of both study periods (Figure 15). There are several values greater than the limit of 300 (high aggressiveness) in all scenarios, especially in the RCP 8.5 scenario and in both periods of the climate scenarios, while a very high value of the index appears in the first period (2031–2060) of scenario RCP 8.5 (about 800).

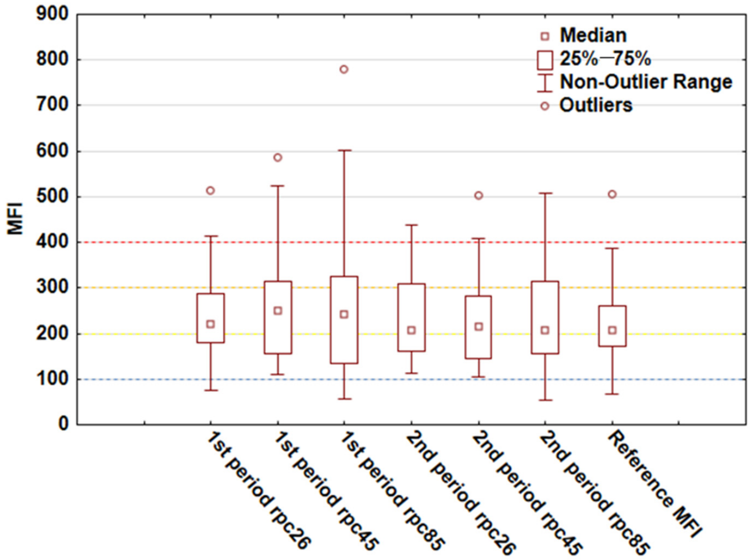

Figure 15. Variance in the distribution of velocity values for the reference period and the climate scenarios. Dashed lines are reference lines indicating the MFI class boundaries as stated in Equation (1).

Thus, the above findings indicate a slight increase in the precipitation aggressiveness in the future, which may increase flood risk, erosion, and damage in archaeological sites.

3.3. Flood Risk

Calculating the flood hazard based on Equation (2) and using the relevant data described in Table 1 together with the average MFI value of the reference period resulted in the flood hazard map that classifies the study area into five flood risk zones (from very low to very high), which are presented in Figure 16. Therefore, it can be seen that areas showing a very high flood risk are a part of the Corfu Old Town (its western edge) and the flat part of the coastal zone near the port and the marina where most of the stormwater is concentrated due to the slopes of the surrounding area. Parts of the coastal zone on the eastern front of the study area and some of the narrow alleys of the old town that appear to have less than optimal conditions for the discharge of rainwater are also at high flood risk (Figure 16). The remaining parts of the old town and Spianada Square show a moderate flood risk (yellow color on the map), while the two castles/fortresses, due to being built on relatively high altitudes, have favorable conditions in terms of slopes and soil cover, and thus, have a very low flood risk.

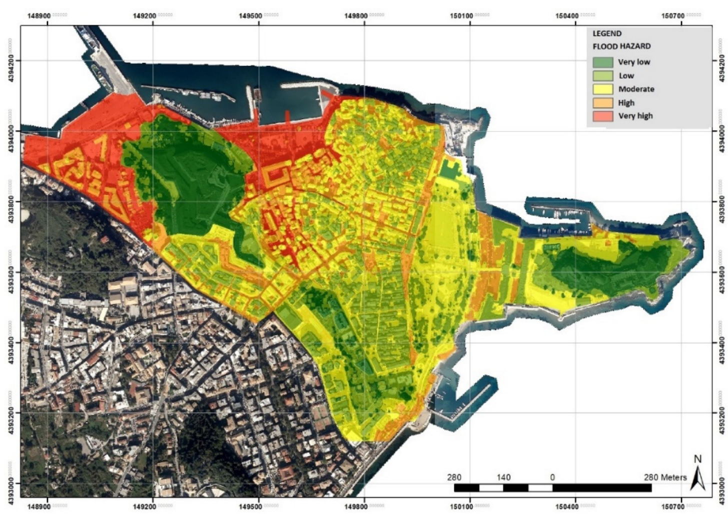

Figure 16. Flood hazard map for the average rain rate of the reference period (1971–2004).

The flood hazard map for the maximum rainfall aggressiveness of the long-term climate scenarios (Figure 17) is similar to the aforementioned flood hazard map for the average rainfall aggressiveness of the reference period, with the main difference being that some areas of the eastern and southern coastal fronts are moved from high to very high flood risk, while Spianada Square has a high flood risk compared to the reference period (moderate risk). In this case, the areas at the western end of the old city and the coastal front near the port marina are also at the greatest risk of flooding.

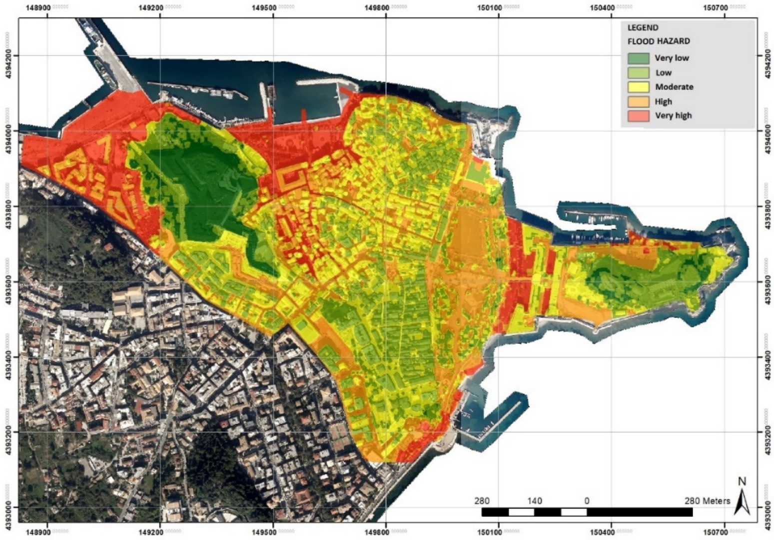

Figure 17. Flood hazard map for the maximum rain rate of the climate scenario (2031–2060, RCP 8.5).

Regarding the flood hazard (combination of flood risk and impact), in both of the MFI cases (average and maximum aggressiveness of rain), the areas that need anti-flood protection measures are the western part of the old city and some other parts of the city that cannot transfer towards the sea a very large amount of water as surface runoff (due to very narrow streets and inappropriate slope directions). The coastal zone on the western and eastern fronts is also at risk of flooding but to a relatively lesser extent and perhaps with lower priority since no significant infrastructure exists there (Figures 18 and 19).

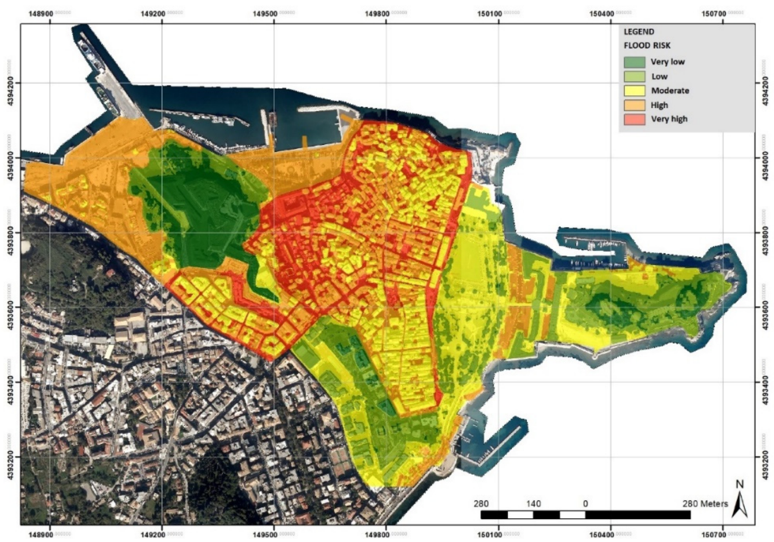

Figure 18. Flood risk map for the average rain rate of the reference period (1971–2004).

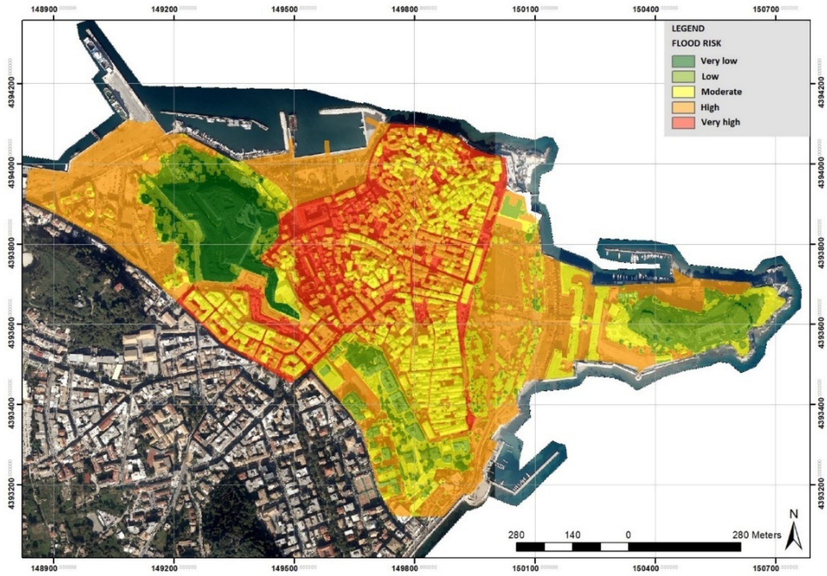

Figure 19. Flood risk map for the maximum rainfall rate of the climate scenario (2031–2060, RCP 8.5).

4. Discussion and Conclusions

In this study, a flood hazard assessment was conducted in a UNESCO world heritage site that is a living monument through multicriteria analysis in GIS software. Even though Corfu Old Town is a coastal area and the low parts of it may be prone to inundation from sea storms and waves, the main flood risk factors are the rainfall amount and intensity since the area receives the highest amount of rainfall in the country. Moreover, this part of Corfu Island is facing eastwards to the nearby shores of Albania and Greece, which create a semi-enclosed gulf that protects the area from large waves and sea storms to a certain degree. Additionally, the hilly topography of the large parts of the old city and the castles is another protective mechanism against floods from both rainfall and sea storms. Nevertheless, there is a very high flood risk for the western part of the old city and the adjacent coastal front up to the port marina, while a very high flood risk was assessed in the future climate scenario for parts of the eastern coastal front as well. This output is in accordance with observations from recent floods that created problems in this particular section of the old town (called Spilia), as reported by the local news.

After analyzing the flood risk for the study area, it emerged that no significant differences are expected in terms of flood risk in the future compared to what was observed in the reference period (1971–2004). Nevertheless, it should be mentioned that there is a degree of uncertainty in this finding because the rainfall data of the climate models were available only at daily time steps and not hourly, which is the ideal temporal scale for urban flood studies. However, such fine-resolution data are not often available even as past measurements, while for climate change scenarios, they are completely absent. The purpose of this study was to assess potential changes between the current and future climate conditions that could lead to an increased flood risk in this specific area in the future. Therefore, at the initial stage, all the different aggregation possibilities of rainfall data and statistics were examined and compared between the reference and future periods and climate scenarios. Emphases were placed on the monthly and annual aggregations that are more likely to occur in relation to the daily values due to the inherent limitations of the long-term climate models. Nonetheless, no significant changes were observed in this comparative assessment, apart from a few extreme daily rainfall values that were estimated under specific climate scenarios (mostly for the period of 2031–206).

A similar approach for flood hazard mapping has been followed by many other researchers [2,3,5,14,15], indicating that it is an efficient approach, especially for areas with a limited availability of high-resolution data (spatial and temporal), and where the implementation of hydraulic modelling is not an option. There are uncertainties involved with this approach, such as the subjectivity of the weighting factors or the accuracy of the climate data, but for comparative risk assessment purposes between the current and future climate conditions for identifying significant changes and hotspots of high-flood-risk areas, it is usually acceptable.

The wider study area is included by the Hellenic Ministry of Environment in the zones of potentially high flood risk, in accordance with the Floods Directive (2007/60/EU, https://floods.ypeka.gr/, accessed on 3 May 2022). Despite this, the flood risk assessment plans of the Ministry have not recorded significant historical floods in the city of Corfu. Nevertheless, the drainage infrastructure of rainwater in the old city is not very efficient, especially in the low-altitude zones where overflows of sewers and drainage pipelines are often observed when the intensity of the rain is very high and the accumulated water cannot be channeled through the storm drains to the sea. Therefore, one of the interventions that should be considered in order to improve the anti-flood protection of the city is to increase the drainage capacity of rainwater pipes where possible, given the limitations for large-scale technical works in the old city.

Additionally, 'smart' solutions could be used to reduce the effects of flood events with the construction of relatively small-scale drainage pipes and/or ditches in parts of the city where it is possible, such as in the periphery of the city, especially towards the fort located in the western part of the study area. In this way, a percentage of the water that flows towards the part of the city with a very high flood risk can be collected and removed in a controlled manner. Nature-based solutions (NBSs) are also compatible with the characteristics of a cultural site, and Kumar [16] assessed different types of tools and models to develop and choose alternative designs of NBSs for mitigating natural hazards.

Additionally, an early warning system that would include automatic weather stations as well as water levels and discharge sensors at key points with high flood risk and within the most basic storm drains would be important to inform the competent authorities and residents to avoid large damage to the economy and threats to human lives. In addition, separate rainwater and sewer pipes should be constructed to stop sewage pipes from overflowing when there is heavy rainfall. Finally, any flood protection effort should be consistent with the character and protection status of the study area and use local knowledge on dealing with flood events, with good practices that may come from the tradition and history of the city.

Funding: This study was conducted under the project 'LIFE-IP AdaptInGR—Boosting the implementation of adaptation policy across Greece LIFE17 IPC/GR/000006', deliverable 'Sub-Action C.4.2: Development of pilot assessments and adaptation guidelines for cultural heritage. Case Study: The Archaeological site of Corfu old town', with the contribution of the LIFE Programme of the European Union and of the Hellenic Green Fund.

Data Availability Statement: Not applicable.

Conflicts of Interest: The author declare no conflict of interest. The funders had no role in the design of the study; in the collection, analyses, or interpretation of data; in the writing of the manuscript; or in the decision to publish the results.

References

1. Mentzafou, A.; Dimitriou, E. Hydrological Modeling for Flood Adaptation under Climate Change: The Case of the Ancient Messene Archaeological Site in Greece. *Hydrology* **2022**, *9*, 19. [CrossRef]
2. Liu, J.; Xu, Z.; Chen, F.; Chen, F.; Zhang, L. Flood Hazard Mapping and Assessment on the Angkor World Heritage Site, Cambodia. *Remote Sens.* **2019**, *11*, 98. [CrossRef]
3. Ortiz, P.; Antunez, V.; Martín, J.M.; Ortiz, R.; Vázquez, M.A.; Galán, E. Approach to environmental risk analysis for the main monuments in a historical city. *J. Cult. Herit.* **2014**, *15*, 432–440. [CrossRef]
4. Lanza, S.G. Flood hazard threat on cultural heritage in the town of Genoa (Italy). *J. Cult. Herit.* **2003**, *4*, 159–167. [CrossRef]
5. Mentzafou, A.; Markogianni, V.; Dimitriou, E. The Use of Geospatial Technologies in Flood Hazard Mapping and Assessment: Case Study from River Evros. In *Geoinformatics and Atmospheric Science*; Niedzielski, T., Migała, K., Eds.; Pageoph Topical Volumes; Birkhäuser: Cham, Switzerland, 2018. [CrossRef]

6. Papageorgiou, M. Planning practices for the protection of cultural heritage: Lessons learnt from the Greek UNESCO sites. *Eur. Spat. Res. Policy* **2015**, *22*, 111–125. [CrossRef]
7. IPCC, Fifth Assessment Report. 2020. Available online: https://www.ipcc.ch/assessment-report/ar5/ (accessed on 2 May 2022).
8. Morgan, R.P.C. *Soil Erosion and Conservation*, 3rd ed.; Blackwell Publishing: Oxford, UK, 2005.
9. Kourgialas, N.N.; Karatzas, G.P. Flood management and a GIS modeling method to assess flood-hazard areas—A case study. *Hydrol. Sci. J.* **2011**, *56*, 212–225. [CrossRef]
10. Gemitzi, A.; Petalas, C.; Tsihrintzis, V.A.; Pisinaras, V. Assessment of groundwater vulnerability to pollution: A combi-nation of GIS, fuzzy logic and decision making techniques. *Environ. Geol.* **2006**, *49*, 653–673. [CrossRef]
11. Schauble, H.; Marinoni, O.; Hinderer, M. A GIS -based method to calculate flow accumulation by considering dams and their specific operation time. *Comput. Geosci.* **2008**, *34*, 635–646. [CrossRef]
12. Varlas, G.; Stefanidis, K.; Papaioannou, G.; Panagopoulos, Y.; Pytharoulis, I.; Katsafados, P.; Papadopoulos, A.; Dimitriou, E. Unraveling Precipitation Trends in Greece since 1950s Using ERA5 Climate Reanalysis Data. *Climate* **2022**, *10*, 12. [CrossRef]
13. Valdés-Pineda, R.; Pizarro, R.; Valdés, J.B.; Carrasco, J.F.; -Chevesich, P.G.; Olivares, C. Spatio -temporal trends of precipitation, its aggressiveness and concentration, along the Pacific coast of South America (36–49°S). *Hydrol. Sci. J.* **2016**, *61*, 2110–2132. [CrossRef]
14. Ravankhah, M.; de Wit, R.; Argyriou, A.V.; Chliaoutakis, A.; Revez, M.J.; Birkmann, J.; Žuvela-Aloise, M.; Sarris, A.; Tzigounaki, A.; Giapitsoglou, K. Integrated Assessment of Natural Hazards, Including Climate Change's Influences, for Cultural Heritage Sites: The Case of the Historic Centre of Rethymno in Greece. *Int. J. Disaster Risk Sci.* **2019**, *10*, 343–361. [CrossRef]
15. Gouett-Hanna, C.; Oulahen, C.; Henstra, D.; Thistlethwaite, J. Flood risk assessment data access and equity in Metro Vancouver. *Can. Water Resour. J. Rev. Can. Des Ressour. Hydr.* **2022**, *47:4*, 202–215. [CrossRef]
16. Kumar, P.; Debele, S.E.; Sahani, J.; Rawat, N.; Marti-Cardona, B.; Alfieri, S.M.; Basu, B.; Basu, A.S.; Bowyer, P.; Charizopoulos, N.; et al. Nature-based solutions efficiency evaluation against natural hazards: Modelling methods, advantages and limitations. *Sci. Total Environ.* **2021**, *784*, 147058. [CrossRef] [PubMed]